

## Applications of the limit theorems<sup>1</sup>

Application of the basic ideas of the limit capacity analysis, assisted by fundamental knowledge of mechanics of materials, leads to simple techniques of bearing capacity assessment. These methods, sometimes very elementary, give significantly good results.

Statically admissible field of stress has to fulfill the equilibrium conditions and do not contradict the yield criterion. The conditions required to establish a lower-bound solution are essentially as follows:

- (1) A complete stress distribution or stress field must be found, everywhere satisfying the differential equation of equilibrium.
- (2) The stress field at the boundary must satisfy the stress boundary conditions.
- (3) The stress field must nowhere violate the yield condition

From these rules it can be seen that a lower-bound technique is based entirely on equilibrium and yield conditions but it must not, however, be confused that the limit equilibrium method or slip-line field gives a lower-bound solution. In these method the stress state is specified only either along the slip lines or in local plastic stress zone around the load and not everywhere in the solid, as required by item (1), and therefore a limit equilibrium solution or a slip-line solution does not give a complete equilibrium solution. Even if a complete equilibrium solution can be found, it remains to be demonstrated that such a stress distribution will not violate the yield condition, as required by item (3).

### Discontinuous fields of stress

Very often, during constructions of admissible stress fields, it is necessary to admit several zones of the stress field. The stress distribution in each zone is homogeneous. At the stress boundaries the stress discontinuities appear. The same discontinuity appears at plastic hinge.

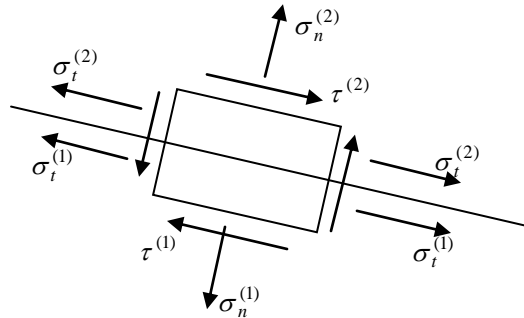


Fig. 4.1 Discontinuity of the normal stress

In marked contrast to the velocity admissible fields where discontinuity is not only useful and convenient in upper-bound calculation but often is contained in actual collapse mode or mechanism, discontinuous stress fields are useful and permissible in lower-bound calculation but are rarely the actual state.

However, these separate fields of stress can be valid if they fulfill the equilibrium conditions at each point of discontinuity. We see from the figure that the equality of normal and shear stress at both sides of the border are required:

$$\sigma_n^{(1)} = \sigma_n^{(2)} \quad \text{and} \quad \tau^{(1)} = \tau^{(2)},$$

while the components  $\sigma_t^{(1)}, \sigma_t^{(2)}$ , parallel to the border, can be different.

### Mohr's diagrams

We shall restrict our discussion to the plane strain condition in which the dimension perpendicular to the plane of the drawing is infinitely long. The velocity components  $v_x$  and  $v_y$  are independent of  $z$ , while  $v_z$  is zero. Under these circumstances, the stress components  $\tau_{yz} = \tau_{zx} = 0$  and the remaining components  $\sigma_x, \sigma_y, \sigma_z$  and  $\tau_{xy}$  are independent of the coordinate  $z$ .

<sup>1</sup> adapted from Lubliner, op. cit.

The vanishing shear stresses indicates that the stress component  $\sigma_z$  is a principal stress and the  $z$ -direction is a principal direction. In the Mohr stress diagram the normal stress and the shearing stress are used as coordinates.

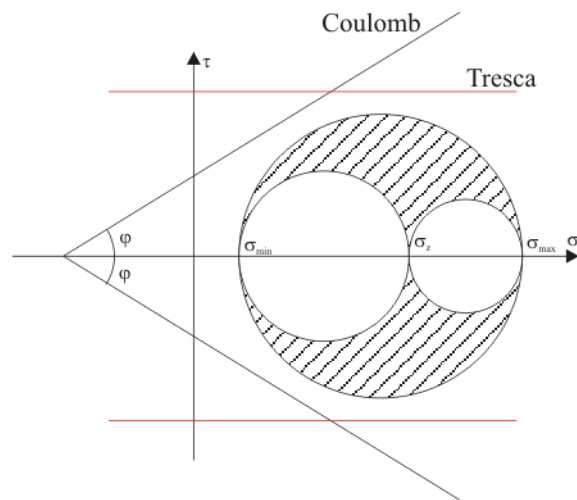


Fig. 4.2 Mohr's circles

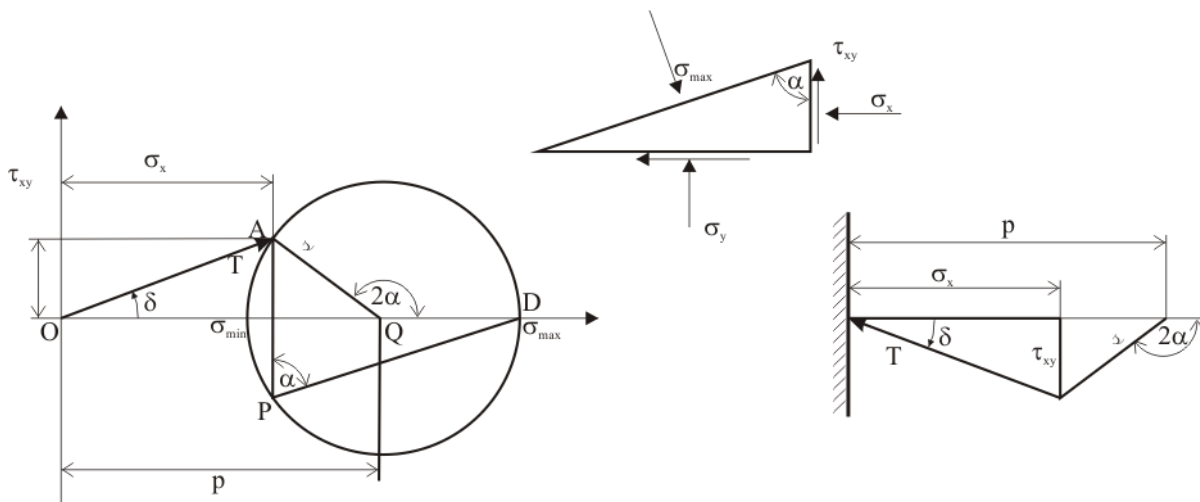


Fig. 4.3 Mohr's circles and their basic features

Values of stresses satisfying the Coulomb or Tresca condition are represented in figure by points in the region inside the straight lines representing the flow surface. Yielding of the material can occur when the largest of the circles touches the lines. In the plane strain condition, instead of a three-Mohr circle representation, it is sufficient to consider only the stress variation in the  $xy$ -plane or the Mohr circle passing through the two points of extreme stresses, and instead of stresses on some element of area, we have only to consider stresses on some linear element.

The point  $A$  in the figure correspond to the surface element the normal  $n$  of which is in the positive  $x$ -direction. On this surface there will be applied an actual stress  $T$  forming an angle  $\delta$  with the normal  $n$  and having normal and tangential components  $\sigma_x, \tau_{xy}$ . The stress vector  $T$  may be also considered as having hydrostatic pressure  $p$  normal to the surface and maximum shear stress component  $s$  forming an angle  $2\alpha$  with the normal  $n$ . In the Mohr diagram sketch the angles are measured positive in the counter-clockwise sense.

It is well known that the central angle of the arc  $AQD$  equals  $2\alpha$ . However, the position of point  $A$  can also be determined without laying off the angles by means of the following procedure. We trace through  $D$  a line parallel to the principal section shown in the inset of the figure. This line intersects

the circle at point  $P$ . This point is called the pole of the Mohr circle. When the pole is known, the point of the circle which corresponds to a given surface element is readily found by drawing, through the pole, a line parallel to the trace of the surface element and determining the second intersection of this line with the circle.

### Sum of two stress fields

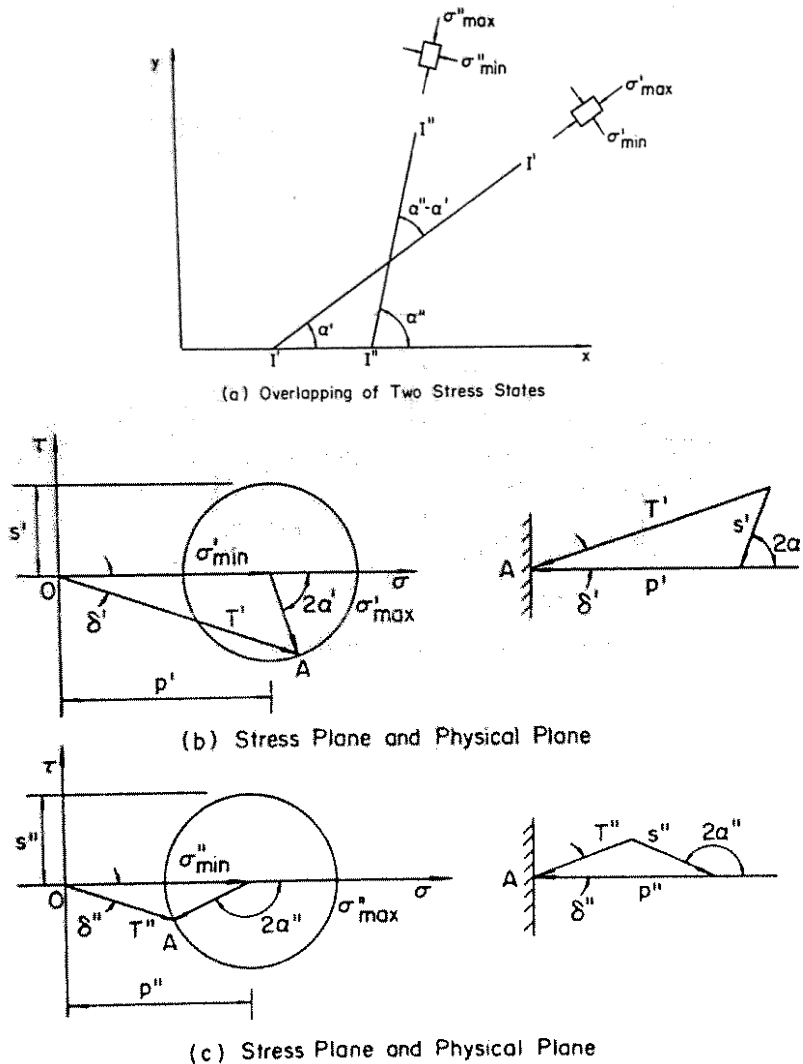


Fig. 4.4 Addition of two stress fields

One of the most important application of the Mohr stress circle method is to solve the following problem: We know the directions and intensities of the principal stresses of several uniform stress fields. We also know the yield condition (Coulomb's or Tresca's). We want to determine whether the resultant stress field obtained from the superposition of these individual stress fields will violate the yield condition. In order to solve our problem it is sufficient to remember that the resultant stress state is determined completely by the values  $p$  and  $s$  corresponding to the resultant components of the resultant traction  $T$  on any section through the point. Since the hydrostatic pressure components  $p'$  and  $p''$  are always perpendicular to the element, the resultant hydrostatic pressure component  $p$  is simply the algebraic summation of the hydrostatic components. However, the resultant shear component  $s$  is the vector summation of the shear components.

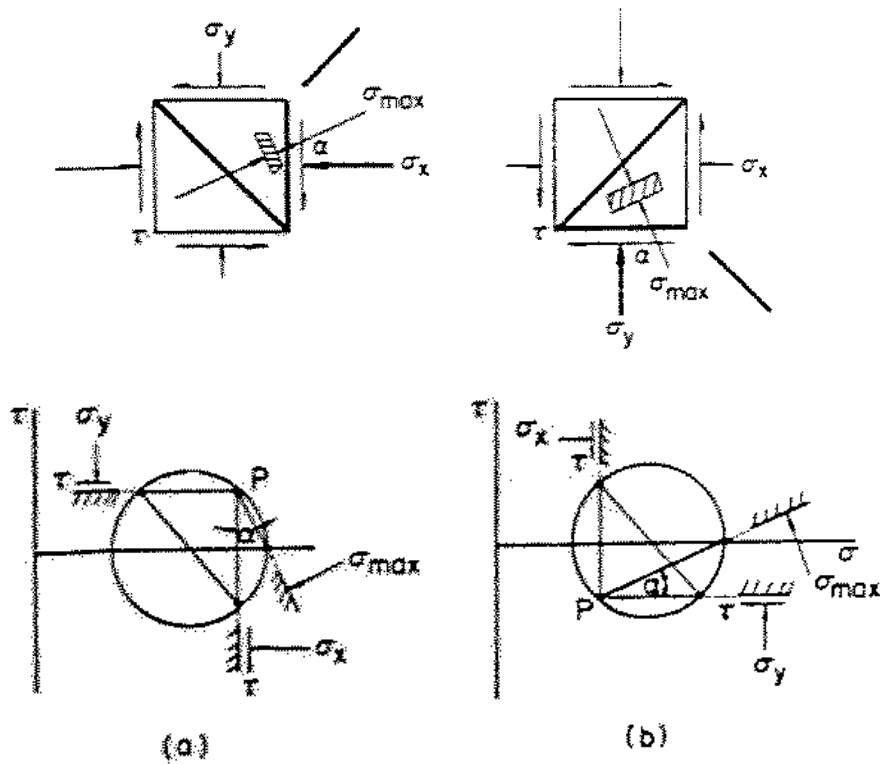


Fig. 4.5 Directions of principal stresses and planes on which they act

Two stress conditions are sketched in the above figure; the purpose of this figure is to demonstrate a direct means of obtaining a physical feeling for states of stress without any calculation or the drawing of Mohr's circle. The combination of normal stresses and the shear one gives a principal stress direction  $\alpha$  between the two extremes of direction as shown, and a corresponding orientation of principal plane between the two extreme plane positions.

It may be advantageous to divide the body into several stress zones. In each zone the stress field will satisfy the equations of equilibrium and not violate the yield condition; further, the stress field will be continuous in each zone. However, the stress state on the boundary between two neighboring zone may not be identical. Here we shall exploit the possibility of discontinuity of stress between two adjacent stress elements at the boundary.

Consideration of the equilibrium of a long and narrow element containing the boundary where the state of stress on either side is denoted by the subscripts  $t$  and  $n$ , tangential and normal to the boundary respectively, shows that in the absence of self-weight of material the normal stress  $\sigma_n$ , and the shear stress  $\tau$ , must be continuous or:

$$\sigma_n^1 = \sigma_n^2 \quad \text{and} \quad \tau^1 = \tau^2$$

where the superscripts denote the zones. Equilibrium, however, places no restrictions on the change of  $\sigma_t$  across the boundary. As far as the equilibrium is concerned we can have a discontinuity in the  $\sigma_t$ -component across the boundary, although the other components of stress,  $\sigma_n$  and  $\tau$ , must be continuous across the boundary from the above equation.

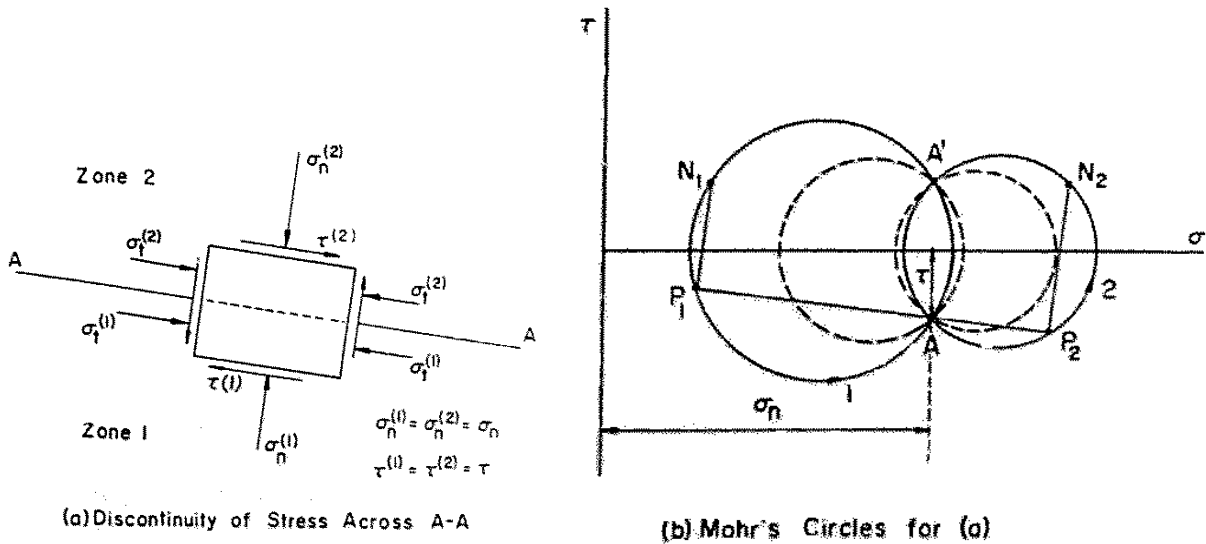


Fig. 4.6 Stress discontinuity and Mohr circles

This situation is illustrated clearly by the Mohr circles for the regions 1 and 2.

The poles of two circles are obtained by drawing a line through A parallel to the element AA of the line of discontinuity. The two stress components  $\sigma_n$  and  $\tau$  coincide at the discontinuous interface A, but the two states of stress, represented by circles 1 and 2 corresponding to two different values of  $\sigma_t$ , may be rather different.

For given values of the normal and shear stresses represented by the point A in the diagram, infinitely many of such circles of various radius can be drawn through A, so as to have their centers on the  $\sigma$ -axis.

In order to obtain a largest lower-bound solution, it is advantageous if the material is at the yield point or plastic stress on both sides of a boundary. In such a case, through A only two circles tangent to the yield lines can be drawn.

Considering, for example, the special case of Tresca material for which  $\varphi = 0$ , the Mohr circles representing limiting states of stress have two parallel lines as an envelope.

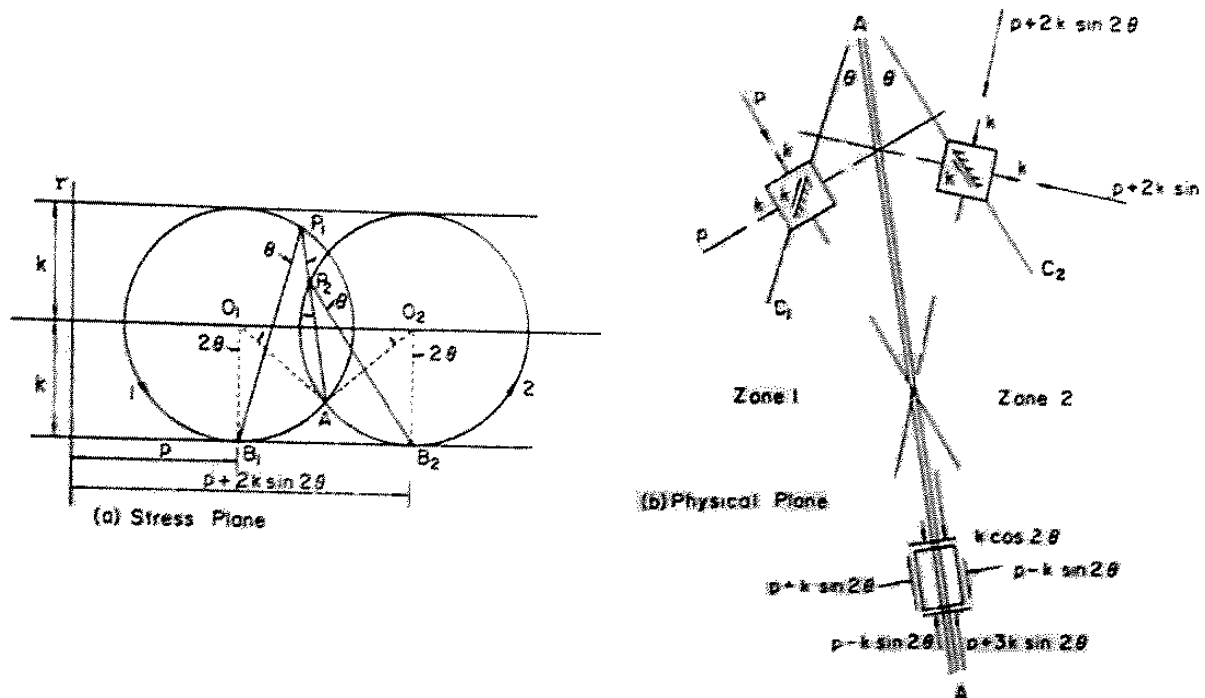


Fig. 4.7 A line of stress discontinuity separating the plastic stress fields 1 and 2 of Tresca material

It follows that the discontinuity line AA must bisect the corresponding directions of principal shear stress on either side of the plastic stress discontinuity. In other words, the axes of principal stresses in the two plastic zones form mirror images of each other in the boundary of stress discontinuity.

**Stretched plate with a hole**

Let's consider a bar with rectangular cross-section  $b \times t$ , stretched by axial force  $P$ , with a hole of diameter  $d$ , located symmetrically. Assume TG yield criterion.

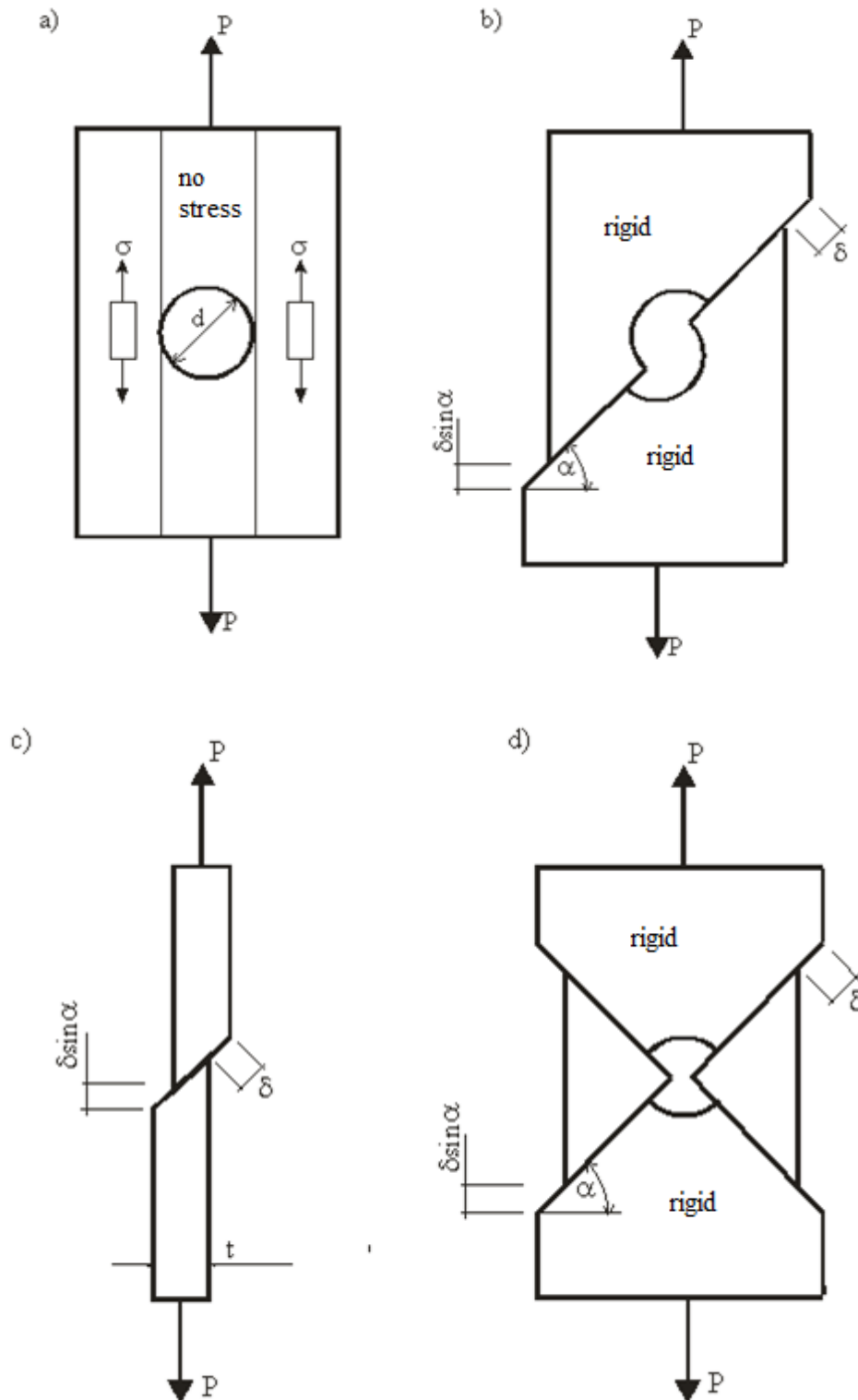


Fig. 4.8 Bar with the circular hole

**Lower bound limit**

The yielding stress for uniaxial tension is  $\sigma_0 = 2\tau_0$ . If there is only one hole, the simplest solution consists from three elongated strips, two of them yielded and third without stress. The lower bound evaluation is:

$$P^D = \sigma_0(b-d)t$$

### Upper bound limit

We seek the kinematically admissible scheme, which fulfill the compatibility conditions. Let's consider three such schemes.

In the first scheme, fig. 1.b, two parts of the bar slide one on one another, crosswise to the hole at an angle  $\alpha$  with the velocity  $\dot{\delta}$ . The speed of relative movement is  $\dot{\delta} \sin \alpha$ . Comparing the dissipation rate of the internal energy with this of external energy, we have:

$$P \dot{\delta} \sin \alpha = \frac{\tau_0 \dot{\delta} (b-d)t}{\cos \alpha} \rightarrow P_1^G = \frac{2\tau_0 (b-d)t}{\sin 2\alpha}$$

The extreme (minimal) value of the load capacity is reached for an angle of  $45^\circ$ :

$$P_1^G = 2\tau_0 (b-d)t = \sigma_0 (b-d)t$$

The result is identical with the previous one, so, the solution is exact.

In the second scheme, fig.1.c, we assume the slip across the bar thickness. Similarly as before, from the dissipation energy comparison, we get:

$$P \dot{\delta} \sin \alpha = \frac{\tau_0 \dot{\delta} (b-d)t}{\cos \alpha} \rightarrow P_2^G = \frac{2\tau_0 (b-d)t}{\sin 2\alpha} = \dots = \sigma_0 (b-d)t$$

so, the same value as before.

Third variant of the kinematic scheme consists on relative movement of four rigid regions, which form something like the "necking". Comparing the rate of dissipation energies, we get:

$$P_3^G (2\dot{\delta} \sin \alpha) = 4\tau_0 \dot{\delta} \frac{b-d}{2} \frac{t}{\cos \alpha} \rightarrow P_3^G = \frac{2\tau_0 (b-d)t}{\sin 2\alpha} = \dots = \sigma_0 (b-d)t$$

Again, we have the same solution.

### Bending of the notched bar

The notched bar is bent by two moments at its ends. Assume the bar width big enough so it can be in the simple bending.

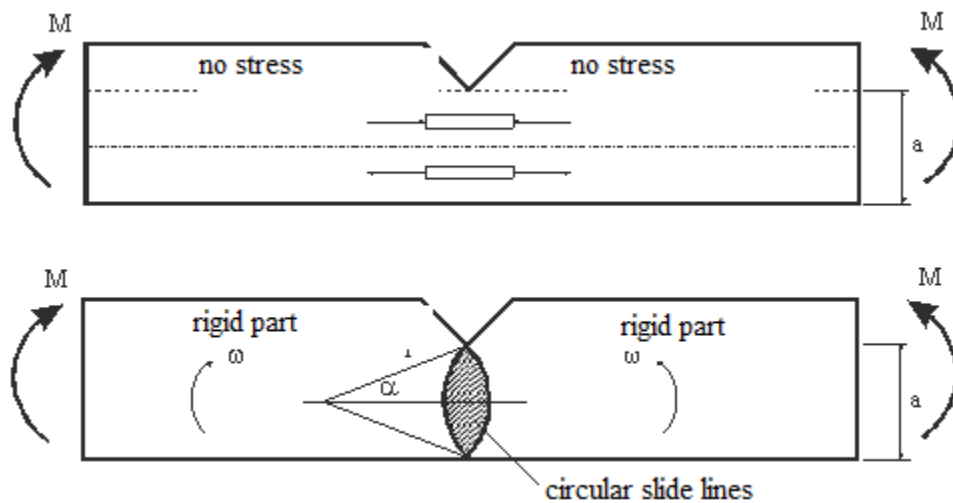


Fig. 4.9 Bending of the notched bar

### Lower bound limit

The stress field composes from three strips with homogeneous stress state. The regions near the notch are without stress and two other carry the bending on: one region in tension and another in compression. Absolute stress value is  $\sigma_0 = 2\tau_0$ :

$$M^D = 2\tau_0 \frac{a}{2} \frac{a}{2} = 0.5\tau_0 a^2$$

### Upper bound limit

The velocity field results from the assumption of rotation round circular hinges with the radius  $r$ . The regions outside and inside the hinges are rigid and not deformed. Comparing the rate of energies, we have:

$$\dot{L}_w = 2\tau_0(r\omega)(2r\alpha) = 4\tau_0 r^2 \alpha \omega = 4\tau_0 \alpha \omega \left( \frac{a}{2 \sin \alpha} \right)^2,$$

$$\dot{L}_z = 2M\omega,$$

and:

$$M^G = \frac{\tau_0 a^2}{2} \frac{a}{\sin^2 \alpha},$$

The minimum of the moment value is reached for  $\tan \alpha = 2a$ , that is for  $\alpha = 67^\circ$ , and:

$$M^G = 0.69\tau_0 a^2.$$

From both estimations we have the solution in the interval:

$$0.5 \leq \frac{M}{\tau_0 a^2} \leq 0.69$$

### Triangular field of the stress

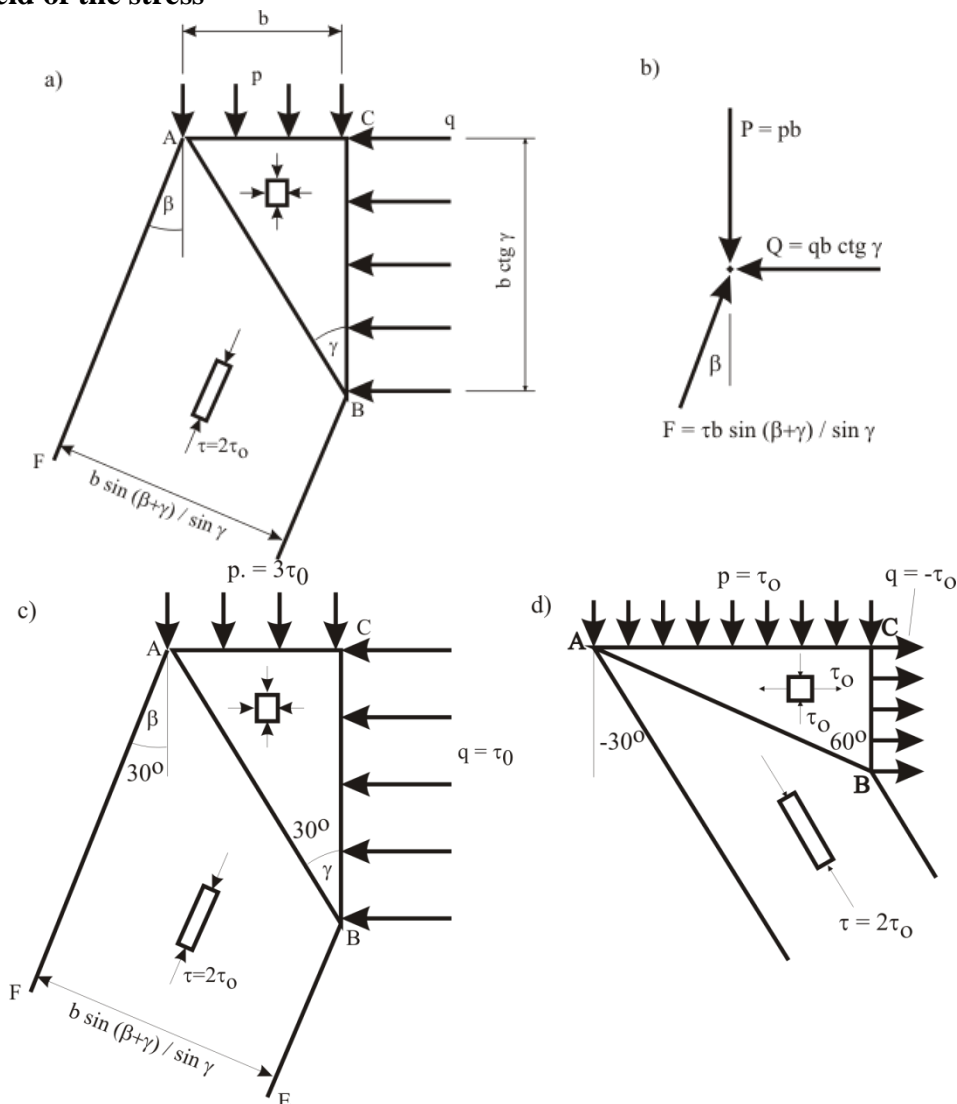


Fig. 4.10 Triangular fields of stress, some cases

If a triangular region is loaded by continuously constant load  $p$  and  $q$  from both sides, fig. 4.a, it is the region of uniform biaxial compression. The region below is – from equilibrium conditions – in the state of simple compression,  $\sigma_0 = 2\tau_0$ .

From fig. 4.b follows that the forces  $P$ ,  $Q$ ,  $F$  must be in equilibrium, so:

$$pb = \frac{2\tau_0 b \sin(\beta + \gamma) \cos \beta}{\sin \gamma} \quad \text{and} \quad qb \cot \gamma = \frac{2\tau_0 b \sin(\beta + \gamma) \sin \beta}{\sin \gamma}.$$

We assume the thickness, perpendicularly to the figure plane, is so important that plane state of stress is valid. For TG yield criterion, the yield criterion in the triangular region will be in the form:

$$p - q = 2\tau_0.$$

Inserting previous terms, we get:

$$\frac{\sin(\beta + \gamma) \cos(\beta + \gamma)}{\sin \gamma \cos \gamma} = 1$$

so

$$\sin 2(\beta + \gamma) = \sin 2\gamma = \sin(\pi - 2\gamma)$$

and

$$\gamma = \frac{\pi}{4} - \frac{\beta}{2}.$$

Substituting last expression to first equations, we have:

$$p = 2\tau_0(1 + \sin \beta), \quad q = 2\tau_0 \sin \beta.$$

The equilibrium at the boundaries is fulfilled because of the balance of the whole set, despite of the normal stress jump parallel to the zones' border.

Fig. 4.c and fig. 4.d present particular cases of such equilibrium.

If  $\gamma = 30^\circ$ , then  $\beta = 30^\circ$  and:

$$p = 3k, \quad q = k, \quad (k \equiv \tau_0).$$

When  $\gamma = 60^\circ$ , then  $\beta = -30^\circ$  and:

$$p = k, \quad q = -k$$

and the triangular region is on biaxial compression and tension..

The case of loading the wedge by continuous constant load on one wall, fig. 4.d (the wedge with an obtuse angle) and fig. 4.e (with an acute angle), can be considered also as a case of a triangular region, which two infinite sides. In the first case, in the triangular region we have biaxial compression and in the second case – biaxial compression and tension.

### Stress fields as truss bars

The triangular stress field is often considered as a set of three truss bars, fig. 5. The loads  $P$  and  $Q$ , triggering biaxial compression in the region, are equilibrated by the force  $F$ . There is no problem of discontinuous stress field if the forces are in equilibrium. The state of stress is simply superposition of the stress applied laterally. If one force is tensile, resulting shearing stress will be much greater than in the first case of both compressed forces.

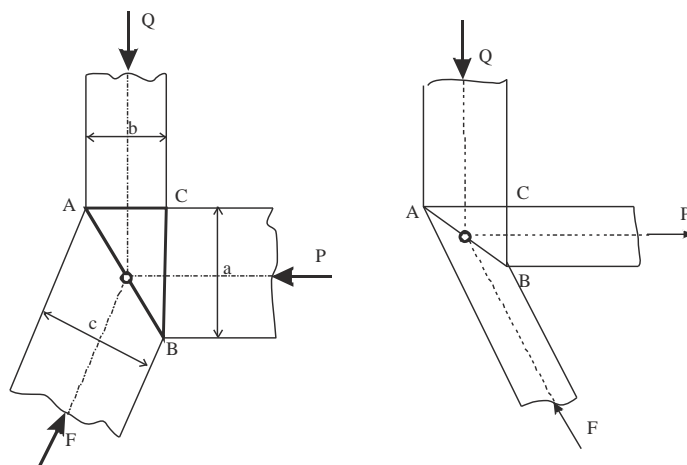


Fig. 4.11 Stress fields as truss bars

### Notched tensioned strip

The figure below presents statically admissible field of stress. The lower bound limit evaluation is:

$$\sigma^D = 1.26\tau_0$$

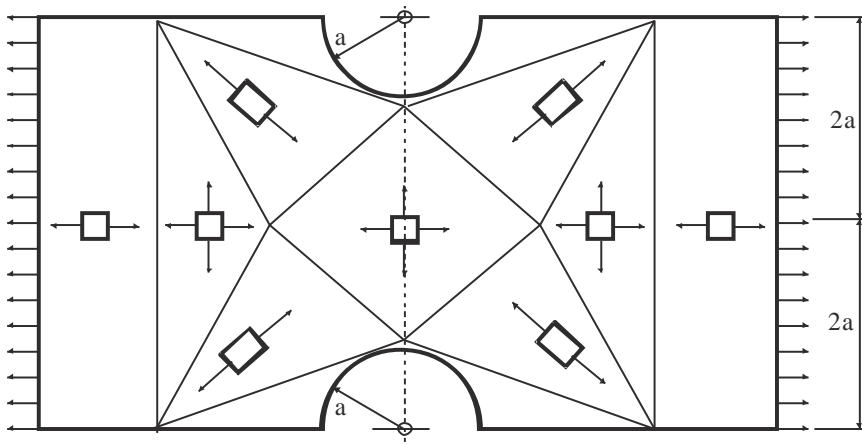


Fig. 4.12 Tensioned strip with notches

**Discontinuous stress fields for cut wedge**

Similar methodology is applied in the case of cut wedge, loaded by uniform continuous load, fig. 6. As before, the truss bars with homogeneous stress state are some part of the region.

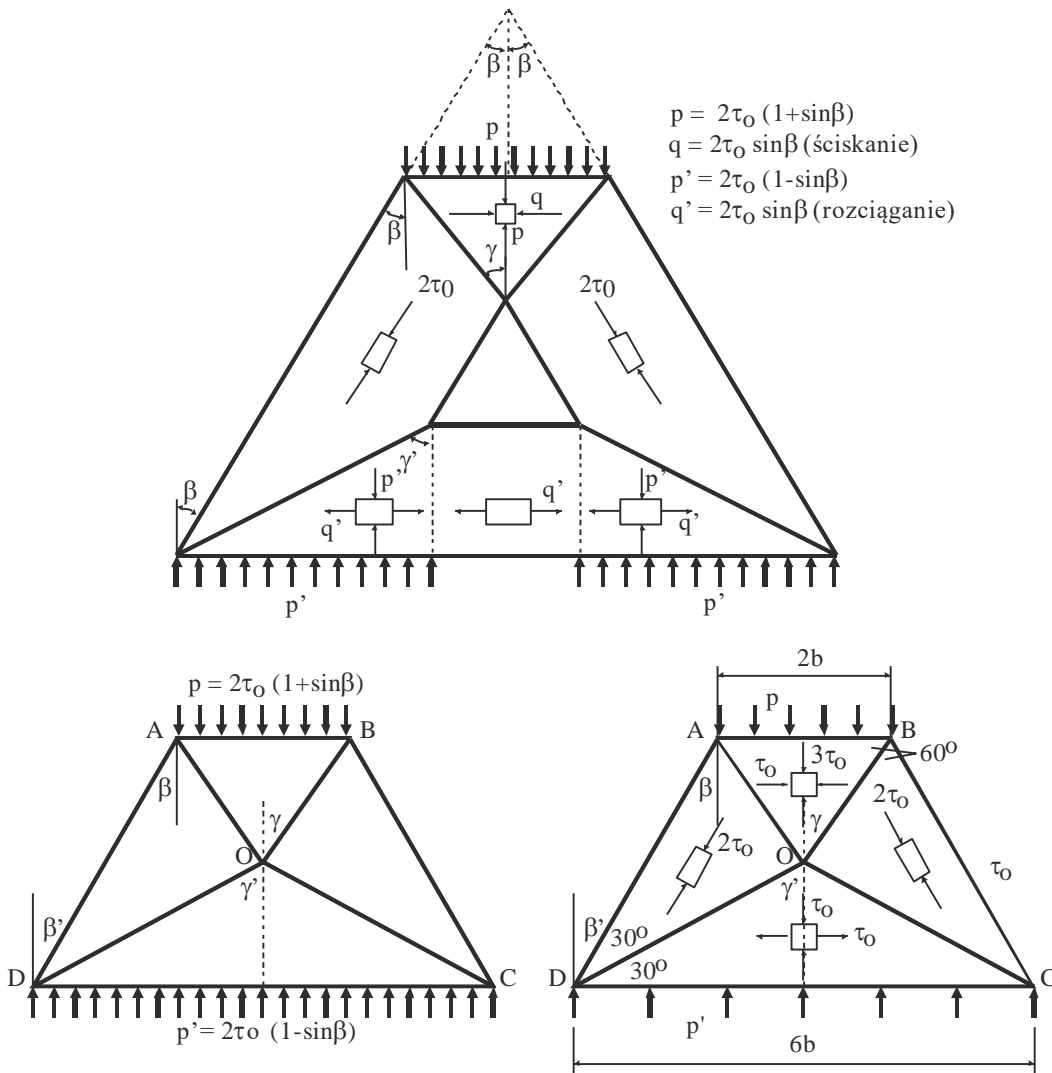


Fig. 4.13 Cut wedge – stress fields

## Indentation – plane state of deformation

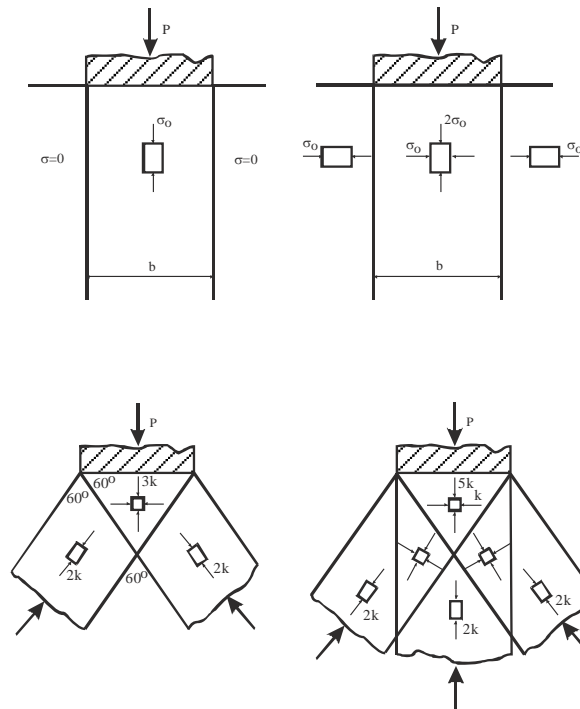


Fig. 4.14 Semi-space punching

Let's consider indentation of rigid stamp into semi-space of perfectly plastic TG material, fig. 8. We assume the plane state of deformation.

As the first approximation, we consider simple discontinuous field of stress under the stamp, for lower bound limit estimation:

$$P_1^D = \sigma_0 b = 2\tau_0 b$$

It is rough evaluation, because of assumption of vertical column of compressed material. To improve the estimation, we add field with horizontal compression on both sides of the column. Then, the region under the stamp is in biaxial compression and the vertical stress can be doubled without yield criterion violation. Adjusted load capacity is:

$$P_2^D = 2\sigma_0 b = 4\tau_0 b$$

As next variant, we use the truss bars method. Assuming two and three bars we consecutively improve the evaluations:

$$P_2^D = 2.5\sigma_0 b = 5\tau_0 b$$

### Upper bound limit estimations – basic methods

The kinematically admissible field of displacements rate, give us upper bound limit of bearing capacity. The method consists on comparison of the rate of energy dissipation. The kinematic field is the collapse scheme that has to be „continuous”: the regions do not overlap nor empty area created. The displacements direction following the kinematic scheme should determine the yield stress used in calculus of dissipation power.

#### Rigid block slide

The figure below presents the simple mechanism of rotation of rigid region round an instantaneous rotation centre. The hinge is created by a line of gliding of two rigid regions one another.

The power of external load is:

$$P(r \cos \theta - \frac{1}{2}b)\dot{\alpha}$$

where  $b$  is the width of the stamp,  $r$  the radius of the hinge,  $\theta$  the angle between the radius of rotation and horizontal surface and  $\dot{\alpha}$  is angular speed of rotation.

The dissipation power is:

$$\tau_0 r (\pi - 2\theta) r \dot{\alpha}$$

from it the estimation follows:

$$P^G = \frac{k(\pi - 2\theta)r^2}{r \cos \theta - \frac{1}{2}b}$$

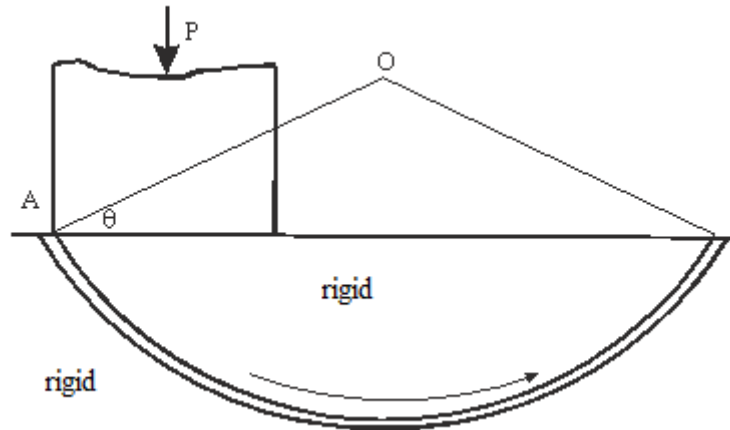


Fig. 4.15 Rigid block slide

Upper bound limit we estimate looking for minimum of the solution for two variables: rotation radius and the angle  $\theta$ :

$$\frac{\partial P^G}{\partial r} = 0 \rightarrow b = r \cos \theta$$

and

$$\frac{\partial P^G}{\partial \theta} = 0 \rightarrow b = r[2 \cos \theta - (\pi - 2\theta) \sin \theta]$$

From the first equation follows that the rotation centre should be on the lateral wall of the block, from the second – by method of trials and errors – we find the angle value:  $\theta = 23.2^\circ$ , finally:

$$P^G = \frac{4\tau_0 b}{\sin 2\theta} = 5.53\tau_0 b$$

### Translation mechanisms

Let's consider the mechanisms of rigid solid translation.

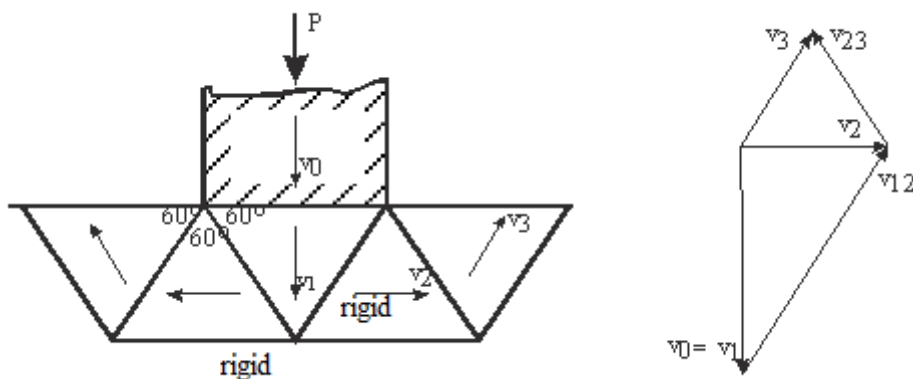


Fig. 4.16 Translation mechanism with friction under the stamp

The first mechanism has a rectangular region, which moves together with the stamp. The graphical presentation of moves of rough stamps and sliding triangular regions is on the figure.

Comparison of the power gives::

$$P^G v_0 = 2\tau_0 \sum l_i v_i = 2\tau_0 b \left( \frac{2}{\sqrt{3}} + \frac{1}{\sqrt{3}} + \frac{1}{\sqrt{3}} + \frac{1}{\sqrt{3}} \right) v_0 \rightarrow P^G = \frac{10\tau_0 b}{\sqrt{3}} = 5.78\tau_0 b$$

For smooth stamp with possible slide under it, fig. 11, we calculate similarly:

$$P^G v_0 = 2\tau_0 \sum l_i v_i = 2\tau_0 \left( \frac{b}{2} + \frac{b}{2} + \frac{b}{2} + \frac{b}{2} + \frac{b}{2} \right) \frac{2v_0}{\sqrt{3}} \rightarrow P^G = \frac{10\tau_0 b}{\sqrt{3}} = 5.78\tau_0 b$$

In both cases the result is the same.

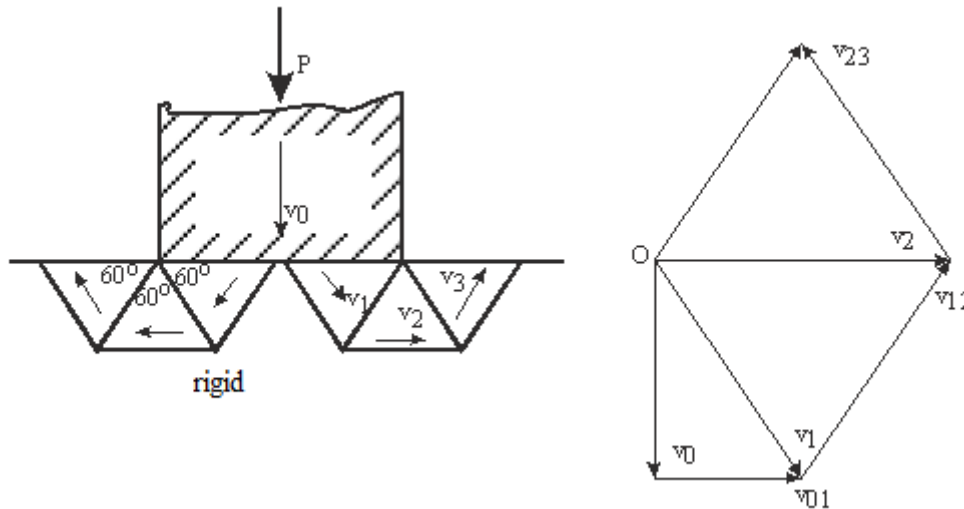


Fig. 4.17 Translation mechanism (without friction under stamp)

### Mixed rotary-translating mechanisms

The example of such mechanism is Prandtl's mechanism and Hill's mechanism.

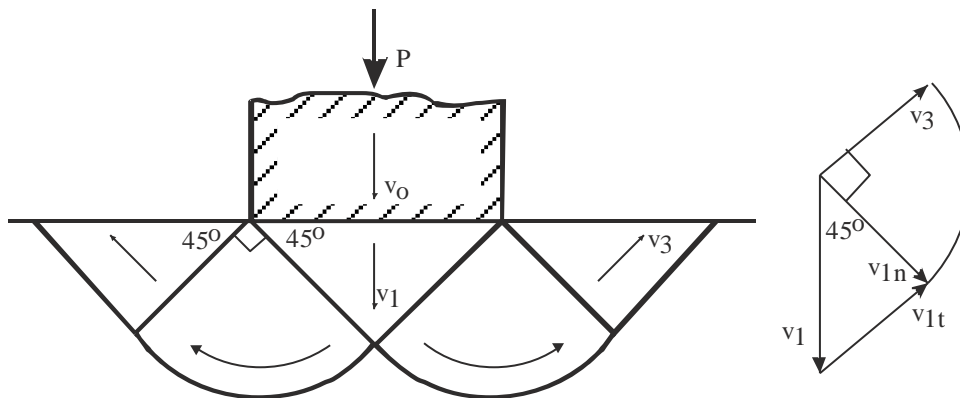


Fig. 4.18 Prandtl's mechanism with friction (1921)

For Prandtl's mechanisms, the dissipation on the straight sliding lines (from the centre to the sides) is:

$$D_1 = \tau_0 \left( \frac{\sqrt{2}}{2} v_0 \right) \left( \frac{\sqrt{2}}{2} b \right) = \frac{1}{2} \tau_0 b v_0, \text{ (straight line)}$$

$$D_2 = \tau_0 \left( \frac{\sqrt{2}}{2} v_0 \right) \left( \frac{\sqrt{2}}{2} b \right) \left( \frac{\pi}{2} \right) = \frac{\pi}{4} \tau_0 b v_0, \text{ (circle)}$$

$$D_3 = \frac{\pi}{4} \tau_0 b v_0, \text{ (straight line)}$$

$$D_4 = \frac{1}{2} \tau_0 b v_0 \text{ (straight line).}$$

Finally:

$$P^G = (2 + \pi) \tau_0 b$$

The same result we get from the Hill's mechanism.

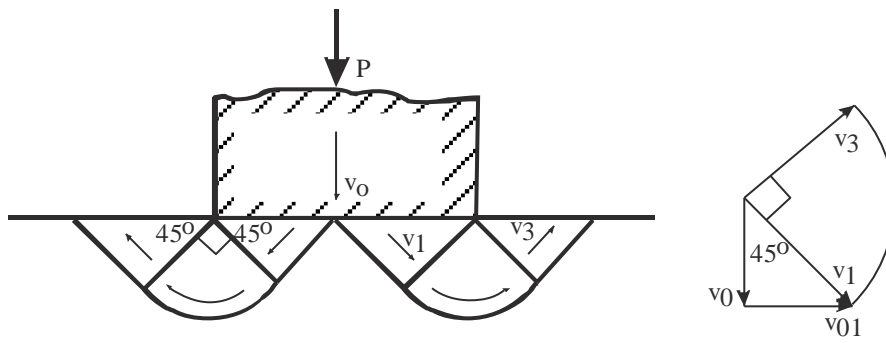


Fig. 4.19 Hill's mechanism with friction under stamp (1950)

If the loading capacity of the material depends on the normal stress (like in the soil), the spiral sliding replace the circular ones. The direction of speed relative to the sliding lines should take into consideration the fact of internal friction angle.

Kinematic schemes of collapse are often an image of real collapse mechanism. This is rarely the case for statically admissible stress fields.